

# Interfacial Effects on Solid Electrolyte Interphase in Lithium-ion Batteries

Zeeshan Ahmad,<sup>†</sup> Victor Venturi,<sup>†</sup> Hasnain Hafiz,<sup>†</sup> and Venkatasubramanian  
Viswanathan<sup>\*,†,‡</sup>

<sup>†</sup>*Department of Mechanical Engineering, Carnegie Mellon University, Pittsburgh,  
Pennsylvania 15213, USA*

<sup>‡</sup>*Department of Physics, Carnegie Mellon University, Pittsburgh, Pennsylvania 15213, USA*

E-mail: venkvis@cmu.edu

## Abstract

The existence of passivating layers at the interfaces is a major factor enabling modern lithium-ion (Li-ion) batteries. Their properties determine the cycle life, performance, and safety of batteries. A special case is the solid electrolyte interphase (SEI), a heterogeneous multi-component film formed due to the instability and subsequent decomposition of the electrolyte at the surface of the anode. The SEI acts as a passivating layer that hinders further electrolyte disintegration, which is detrimental to the Coulombic efficiency. In this work, we use first-principles simulations to investigate the kinetic and electronic properties of the interface between lithium fluoride (LiF) and lithium carbonate ( $\text{Li}_2\text{CO}_3$ ), two common SEI components present in Li-ion batteries with organic liquid electrolytes. We find a coherent interface between these components that restricts the strain in each of them to below 3%. We find that the interface causes a large increase in the formation energy of the Frenkel defect, generating Li vacancies in LiF and Li interstitials in  $\text{Li}_2\text{CO}_3$  responsible for transport. On the other hand, the

Li interstitial hopping barrier is reduced from 0.3 eV in bulk  $\text{Li}_2\text{CO}_3$  to 0.10 or 0.22 eV in the interfacial structure considered, demonstrating the favorable role of the interface. Controlling these two effects in a heterogeneous SEI is crucial for maintaining fast ion transport in the SEI. We further perform Car-Parrinello molecular dynamics simulations to explore Li ion conduction in our interfacial structure, which reveal an enhanced Li ion diffusion in the vicinity of the interface. Understanding the interfacial properties of the multiphase SEI represents an important frontier to enable next-generation batteries.

## Introduction

Lithium-ion (Li-ion) batteries have revolutionized consumer electronics and road transportation<sup>1,2</sup> and offer a promising route to achieve electric aviation.<sup>3-5</sup> The interface between the electrode and the electrolyte in a battery, and the related interphases formed, strongly influence the Coulombic efficiency, cycling performance, and power capability of the battery.<sup>6,7</sup> The properties of a surface or an interface can be vastly different from those of the bulk material. For example, lithium iodide doped with alumina has a Li-ion conductivity orders of magnitude higher than any of the individual components<sup>8</sup> due to the space charge effect. Most solid and liquid electrolytes are not electrochemically or chemically stable at the potentials encountered at the interfaces in Li metal batteries.<sup>9</sup> An ultrathin multicomponent interphase, commonly referred to as solid electrolyte interphase (SEI), first introduced by Peled,<sup>10</sup> is frequently generated as a result of both liquid and solid electrolyte decomposition in Li-ion batteries. Zhu et al.<sup>11</sup> studied the voltage stability windows of some common inorganic solid electrolytes and found that none of them are thermodynamically stable against Li metal anode and form compounds such as LiF,  $\text{Li}_2\text{O}$ ,  $\text{Li}_2\text{S}$ ,  $\text{Li}_3\text{P}$  and  $\text{Li}_3\text{N}$  at the low voltages encountered at anode. The SEI plays a major role in kinetically stabilizing the interface and preventing continued electrolyte decomposition, which can lower the Coulombic efficiency. Several studies have demonstrated a drastic improvement in battery performance

by engineering the SEI, including enabling high energy density Li-metal anodes.<sup>12–16</sup>

With organic liquid electrolytes, the SEI is composed of an inner dense (closer to anode) and an outer porous layer.<sup>17</sup> The passivating film is formed immediately as the anode is placed in contact with the electrolyte. The inner dense layer is composed of crystalline components such as  $\text{Li}_2\text{CO}_3$ ,  $\text{LiF}$  and  $\text{Li}_2\text{O}$  while the outer layer is composed of organic materials.<sup>9</sup> Recent direct operando observations have also confirmed the existence of an inorganic SEI composed mainly of  $\text{LiF}$  and  $\text{Li}_2\text{CO}_3$ .<sup>18</sup> Typically, it is desired that the SEI should allow the movement of Li-ions but be electronically insulating. Its thickness is determined by the electron tunneling range beyond which electrolyte decomposition stops.<sup>19</sup> As Li ion transport through the SEI is often the rate limiting step,<sup>20</sup> understanding ion transport through it is crucial for improving the power capability of the battery. Furthermore, the uniform current density necessary throughout the anode-SEI interface for smooth electrodeposition in Li-metal batteries requires the existence of an SEI layer with homogeneous properties. Several modeling studies have explored the role of interfaces between electrolytes/SEI and the electrode in determining stability, kinetics, charge transfer, and wettability in Li-ion batteries.<sup>21–26</sup> The interfaces within the components of the mosaic SEI, on the other hand, may also hinder or enhance the ion transport in a Li-ion battery. Zhang et al.<sup>27</sup> proposed the synergistic effect between  $\text{LiF}$  and  $\text{Li}_2\text{CO}_3$  as the cause of efficient ion conduction in the SEI. They argued that the presence of two phases,  $\text{LiF}$  and  $\text{Li}_2\text{CO}_3$  promotes ion transport in  $\text{Li}_2\text{CO}_3$  through the formation of interstitial Li in  $\text{Li}_2\text{CO}_3$ . This was backed by calculations of defect formation energies in the bulk phases of  $\text{LiF}$  and  $\text{Li}_2\text{CO}_3$ . However, new questions arise about the role of interfaces in promoting formation of defects and ion transport. Various mechanisms of enhancement of ion conduction due to space charge effects have been proposed<sup>28,29</sup> and exploring the role of heterointerfaces through first-principles might shed more light on intricate physics of ion transport.

In this work, we perform an in-depth study of the effect of interfaces on Li ion hopping, defect formation, electronic transport, and dynamics by explicitly modeling interfaces be-

tween the two major components of the inner SEI layer: LiF and Li<sub>2</sub>CO<sub>3</sub>. We find that the interface causes an increase in the formation energy of the defects, namely Li vacancies in LiF and Li interstitials in Li<sub>2</sub>CO<sub>3</sub> that are responsible for ion transport in the SEI. The activation energy for Li ion hopping in Li<sub>2</sub>CO<sub>3</sub> based on the knockoff mechanism is lowered by the interface. Molecular dynamics simulations are used to calculate the directional activation energies, showing the lowest activation energy of Li ion hopping along [010] direction of Li<sub>2</sub>CO<sub>3</sub>.

## Computational Methodology

### Density Functional Theory calculations

Density functional theory (DFT) calculations were performed using Quantum Espresso plane wave `pw.x` code.<sup>30,31</sup> The Perdew–Burke–Ernzerhof (PBE) exchange–correlation functional was used for all DFT calculations. Energy cutoffs were at least 40 Ry for the wavefunction and 320 Ry for the electron density. Ultrasoft pseudopotentials from the GBRV library<sup>32</sup> were used for Li, C, O and F. These calculations were used to optimize the structures (lattices and ionic positions) of LiF and Li<sub>2</sub>CO<sub>3</sub> as well as the interface between the two for use in molecular dynamics simulations. These calculations were also used to obtain the defect formation energies.

For the calculation of hopping barriers, we used the nudged elastic band (NEB) method<sup>33</sup> as implemented in the projector augmented wave (PAW) package GPAW.<sup>34</sup> Ionic relaxation was performed with a force convergence criterion  $< 0.05$  eV/Å. The atomic simulation environment<sup>35</sup> was used for structure manipulation along with the interface to GPAW and the VESTA package<sup>36</sup> was used for visualization.



## Molecular Dynamics simulations

First-principles Car-Parrinello molecular dynamics<sup>37</sup> simulations were performed using the `cp.x` code in Quantum Espresso.<sup>30,31</sup> We used a time step of 6 au (0.145 fs) with an effective electron mass of 500 au for the electron. The kinetic energy cutoffs used for wavefunction and charge density used were 30 Ry and 300 Ry respectively. The molecular dynamics simulations were performed at temperatures of 600, 800 and 900 K. The DFT-optimized interface was used as the initial structure for the molecular dynamics simulations. A random displacement was then introduced in the ionic positions. The conjugate gradient electron dynamics was used initially and then periodically to bring the electrons on the Born-Oppenheimer surface. The temperature was increased to the required value by setting up a Nose-Hoover thermostat chain<sup>38-40</sup> over a time of  $\sim 7$  ps. The production runs involving diffusivity calculations were done using the microcanonical ensemble to prevent the thermostat from affecting the trajectory.<sup>41</sup> In this work, we only consider the diffusivity of Li atoms in  $\text{Li}_2\text{CO}_3$  since  $\text{Li}_2\text{CO}_3$  is contains relatively more mobile Li ions (activation energy of hopping much lower) and is primarily responsible for conduction. This approach allows us to circumvent any effects that the low number of LiF layers used in the simulation may have on our final results.

## Results and Discussion

### Structure of the Interface

LiF exists in the rocksalt structure (space group 225,  $\text{Fm}\bar{3}\text{m}$ ) with a mixture of edge and corner sharing  $\text{LiF}_6$  octahedra. From DFT calculations, we obtain its lattice constant  $a = 4.0657 \text{ \AA}$ , which agrees well with the experimental value of  $4.0173 \text{ \AA}$ .<sup>42</sup>  $\text{Li}_2\text{CO}_3$  crystallizes in the monoclinic structure with space group 15,  $\text{C}2/c$  with planar  $\text{CO}_3^{2-}$  groups separated by  $\text{Li}^+$  ions. Our computed lattice parameters for  $\text{Li}_2\text{CO}_3$  are  $a = 8.369 \text{ \AA}$ ,  $b = 5.013 \text{ \AA}$ ,  $c = 6.345 \text{ \AA}$ ,  $\alpha, \gamma = 90^\circ$  and  $\beta = 114.093^\circ$  in close agreement with experimental values.<sup>43,44</sup>

A unique interface between LiF and Li<sub>2</sub>CO<sub>3</sub> is identified by the Miller indices of the surfaces of the two materials facing the interface and the two lattice vectors along the interface. We generate a coherent interface by aligning the lattice vectors of LiF and Li<sub>2</sub>CO<sub>3</sub> with angle 90° between them and repeating the in plane lattice vectors. The lowest index (001) surface of LiF is placed parallel to the plane of the interface. Among the low index surfaces, this leaves the choice of (001) or (100) surface of Li<sub>2</sub>CO<sub>3</sub> in plane of the interface. Of these, the (001) surface resulted in lower strain/smaller lattice matched unit cell and was chosen for the simulations. The *c* axis of Li<sub>2</sub>CO<sub>3</sub> is perpendicular to the interface. Considerations of coherency strain minimization and computational tractability led to the following multiplicities of the conventional unit cell lattice vectors: (1, 4, 2) for Li<sub>2</sub>CO<sub>3</sub> and (2, 5, 1) for LiF. These supercells resulted in a coherency strain of less than 3 % for LiF and less than 2 % for Li<sub>2</sub>CO<sub>3</sub>. Li, O or C terminations are possible for the Li<sub>2</sub>CO<sub>3</sub> (001) surface, out of which we chose the Li termination to prevent breaking the C-O bonds. This termination breaks one Li-O bond per Li and reduces the number of Li-O bonds for the surface Li atoms from 4 to 3.

The interfacial distance between the two solids was obtained through energy minimization in two steps: first, single point energy calculations at different values of the distances were performed. This procedure gave a value of  $\sim 3.34$  Å for the distance between the closest Li layers of LiF and Li<sub>2</sub>CO<sub>3</sub>. Finally, using this distance we relaxed the lattice parameters (in the plane of the interface) and the ionic positions using convergence criteria for forces  $< 0.001$  Ry/Å and energy  $< 0.0001$  Ry. The relaxed interface geometry is shown in Fig. 1. For molecular dynamics calculations, only one repetition along z-axis (perpendicular to the interface) for both unit cells was used. The Li-O bonds on an average become shorter at the surface of Li<sub>2</sub>CO<sub>3</sub> compared to the bulk on relaxation.

The interface between LiF and Li<sub>2</sub>CO<sub>3</sub> in the SEI consists of undercoordinated atoms and hence, may be expected to host defects. Zhang et al.<sup>27</sup> proposed the following defect exchange reaction at the interface between LiF and Li<sub>2</sub>CO<sub>3</sub> for the enhancement of Li ion

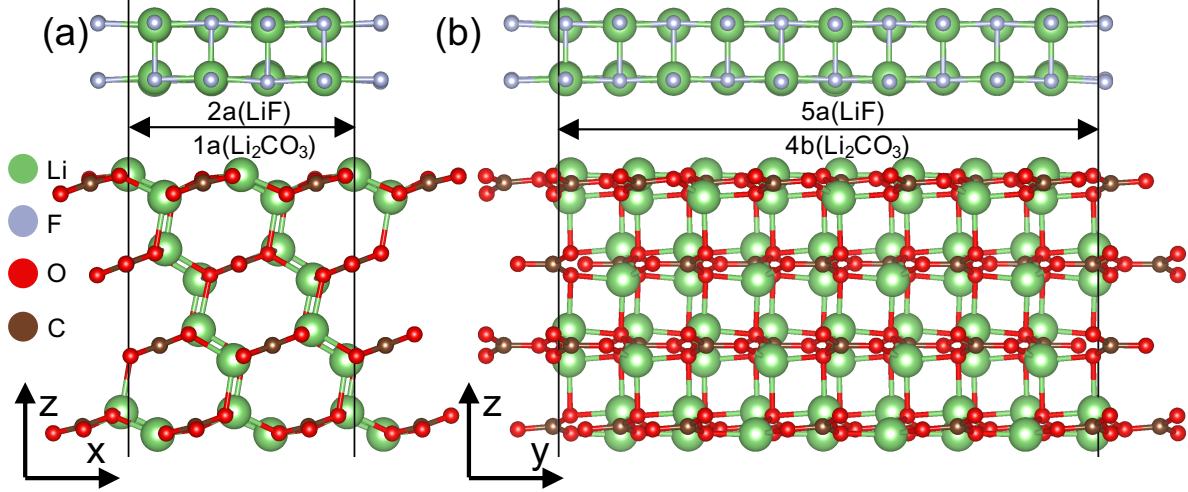
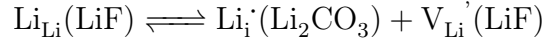


Figure 1: Geometry of the coherent interface between (001) LiF surface and (001) Li<sub>2</sub>CO<sub>3</sub> surface used in DFT calculations. (a) Front and (b) side views along with the axes orientation. The black line is the boundary of the interfacial unit cell used in the simulations with the  $z$  axis is perpendicular to the interface. The coherent interface was generated by using a (2,5,1) supercell of LiF and (1,4,2) supercell of Li<sub>2</sub>CO<sub>3</sub> as shown, resulting in a coherency strain of less than 3 %.

conductivity of Li<sub>2</sub>CO<sub>3</sub>:



Based on defect formation energies and chemical potentials of interstitial Li and Li vacancy in bulk LiF and Li<sub>2</sub>CO<sub>3</sub>, they obtained this as the only favorable reaction (-0.95 eV net energy change). The explicit treatment of the interface allows us to study the initial stage of this reaction when a Li atom migrates from LiF to Li<sub>2</sub>CO<sub>3</sub>, forming an interstitial defect in Li<sub>2</sub>CO<sub>3</sub> and Li vacancy in LiF. This state is shown in Fig. 2. The Li vacancy is circled in yellow and the Li interstitial is shown as a yellow atom in Li<sub>2</sub>CO<sub>3</sub>. The interstitial Li atom relaxes to a configuration with five Li-O bonds similar to lowest energy site II in Ref. 45. The energy required to move a Li ion from LiF to Li<sub>2</sub>CO<sub>3</sub>, hence generating a Li vacancy in LiF and an interstitial Li in Li<sub>2</sub>CO<sub>3</sub> can be calculated as:

$$\Delta E = E_{\text{def}} - E_{\text{pris}} \quad (1)$$

where  $E_{\text{def}}$  is the energy of the defective system and  $E_{\text{pris}}$  is the energy of the pristine

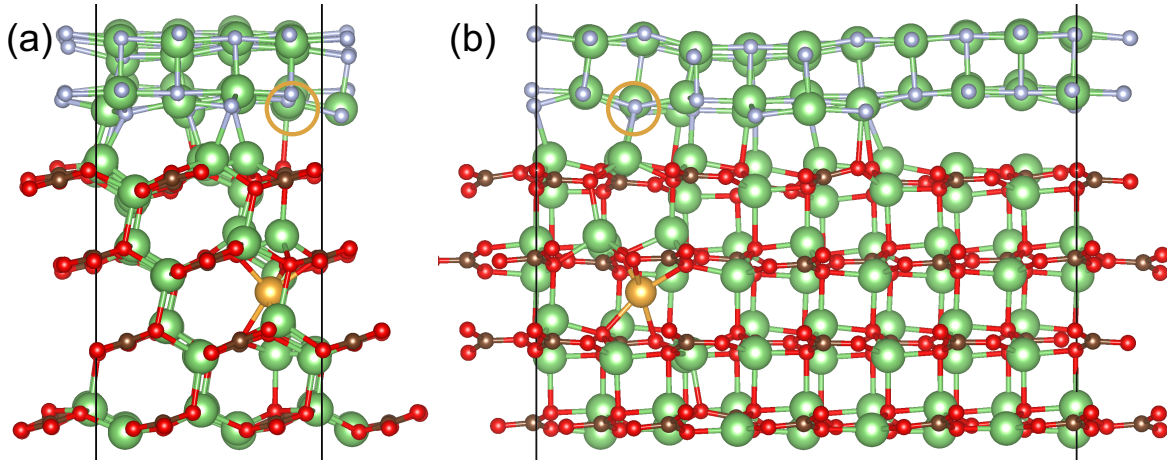


Figure 2: (a) Front and (b) side views of defective structure of the interface between LiF and Li<sub>2</sub>CO<sub>3</sub>. A Li ion from LiF has moved to Li<sub>2</sub>CO<sub>3</sub> creating an interstitial defect in Li<sub>2</sub>CO<sub>3</sub> (yellow atom) and a Li vacancy in LiF (circled in yellow).

system. Our interface calculations show that the energy required to move a Li ion from LiF to Li<sub>2</sub>CO<sub>3</sub> in the configuration shown in Fig. 2 is 1.05 eV. This is an intermediate stage of movement of the defects into the bulk of these solids. The distance between the Li vacancy and interstitial in this Frenkel pair is approximately 7 Å. A smaller separation distance may result in a lower formation energy due to electrostatic attraction, however, we were unable to relax the Frenkel pair located any closer due to the relaxation to the pristine configuration. Our result shows that although the defect exchange reaction is favorable in the bulk, there is a significant barrier in the process as the Li ion moves from the interface towards the bulk of Li<sub>2</sub>CO<sub>3</sub>.

## Electronic Properties

Recently, electronic conductivity of interface between electrode and electrolyte has been proposed as the cause of dendrite growth in solid electrolytes.<sup>46,47</sup> The enhanced dendrite growth at higher temperatures observed by Han et al.<sup>46</sup> points to an important role of electronic leakage through interfaces in promoting dendrite growth. We performed DFT calculations to obtain the electronic density of states (DOS) of the pristine and defective interfacial structures. Figure 3 compares the electronic DOS for the pristine structure and

the one that contains an interstitial Li in  $\text{Li}_2\text{CO}_3$  from LiF. We find that the valence band minimum (VBM) is primarily composed of O 2p states from  $\text{Li}_2\text{CO}_3$  in both cases. The interstitial Li causes distortion of the O atoms in  $\text{Li}_2\text{CO}_3$  and creates a more diffuse O 2p DOS near the VBM. This is in contrast to the results for a Li vacancy in  $\text{Li}_2\text{CO}_3$  which results in formation of localized holes near the VBM.<sup>48</sup> The electron densities for the two cases are compared in Fig. S3 of the Supporting Information. The PBE band gap reduces from 4.97 eV in the pristine structure to 4.48 eV for the defective structure. Although this is a lower bound on the band gap as is expected from semilocal DFT, we do not expect a drastic change in the occupied VBM states by incorporating a Hubbard U for O.<sup>49</sup> Fig. S2 show the contribution of the interstitial Li states to the DOS mainly at the conduction band minimum, causing a reduction of the band gap in the defective structure. The electronic DOS results show that electronic transport through the SEI even in the presence of these heterointerfaces is very small.

## Li Hopping Barrier

Various mechanisms of Li hopping in SEI components have been proposed. Chen et al.<sup>48</sup> performed a study of Li hopping mechanisms in the SEI components LiF,  $\text{Li}_2\text{O}$  and  $\text{Li}_2\text{CO}_3$  in the presence of Li vacancies. However, an exhaustive study of the possible point defects and transport mechanisms in  $\text{Li}_2\text{CO}_3$  found that Li interstitials have the lowest formation energy and are responsible for transport, especially at the anode side.<sup>50</sup> The most favorable pathway for ionic motion in this system is by the *knock-off* or “interstitialcy” mechanism, a form of indirect motion in which an interstitial atom displaces an atom in a lattice site into a neighboring interstitial site, and occupies the now vacant lattice site. The authors argue that, by maintaining a high cation-anion coordination number through all stages of motion, the knock-off mechanism lowers the barrier associated with ion transport when compared to a direct interstitial pathway. Here, we study the effect of the interface between LiF and  $\text{Li}_2\text{CO}_3$  on Li hopping in the latter. Fig. 4 shows the energy landscape of the Li interstitial in  $\text{Li}_2\text{CO}_3$

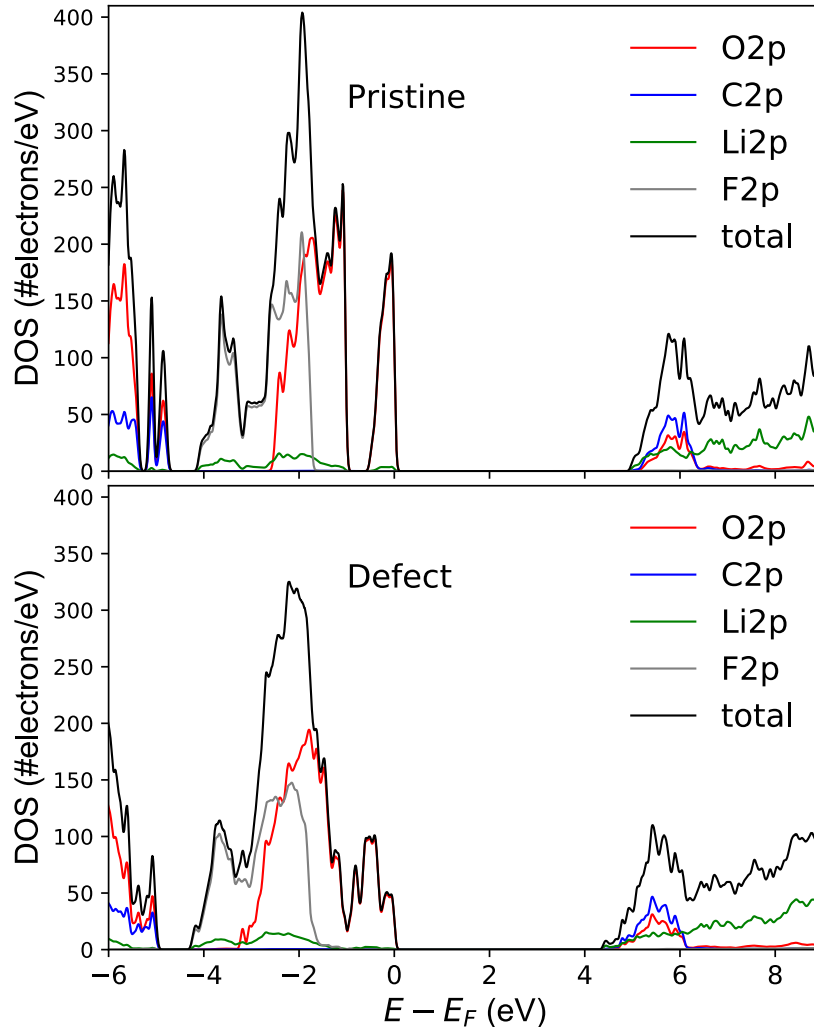


Figure 3: Density of states for the pristine and defective structure of the interface between LiF and  $\text{Li}_2\text{CO}_3$ . The Fermi level ( $E_F$ ) is set to VBM. Notably, no defect states in the band gap are found. The O 2p orbital DOS becomes diffuse due to distortion caused by the interstitial Li in  $\text{Li}_2\text{CO}_3$ . The Li interstitial defect causes a reduction in the PBE band gap by 0.49 eV.

near its interface with LiF based on this knock-off Li transport. Note that the first and the final hopping stages are not equivalent: given that the intended Li motion happens along the [011] direction, the initial interstitial atom has to be placed further from the interface than in the final configuration, as shown in the insets of Fig. 4. The activation energy required to move an atom from one of these interstitial sites to another is thus dependent on the original site, and can be either 0.10 or 0.22 eV. Therefore, the average hopping barrier associated with a net motion pathway parallel to the LiF-Li<sub>2</sub>CO<sub>3</sub> interface is of  $\sim 0.16$  eV. The same knock-off mechanism in bulk Li<sub>2</sub>CO<sub>3</sub> has an activation energy of 0.3 eV,<sup>45</sup> further reinforcing the hypothesis that Li transport is enhanced at the interface of LiF and Li<sub>2</sub>CO<sub>3</sub>. The activation energy is also much lower than that for Li hopping at a surface of LiF (0.34 eV).<sup>51</sup>

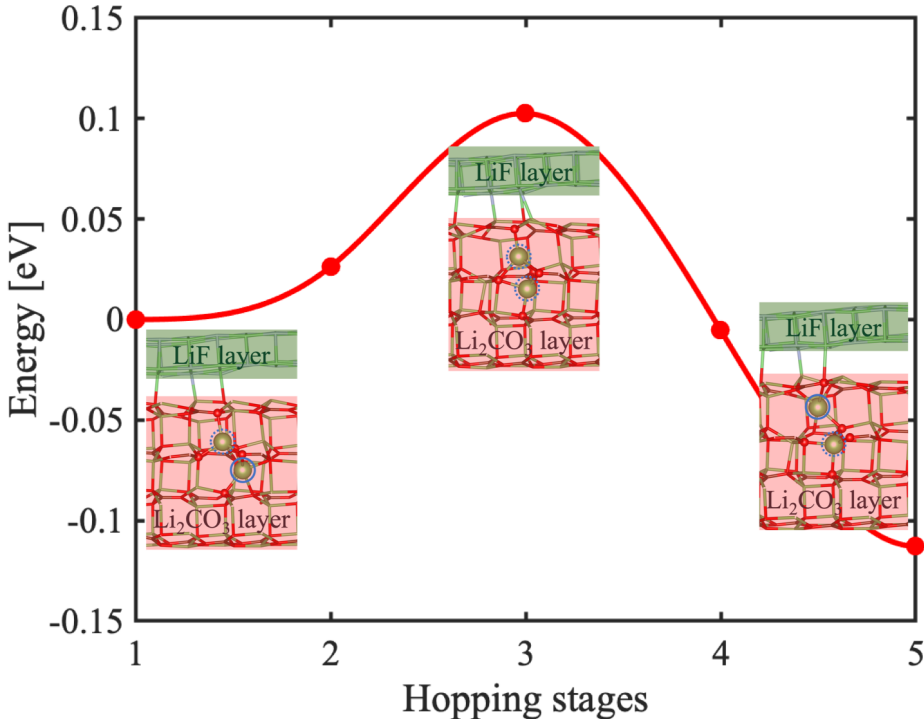


Figure 4: Energetics of minimum energy pathway of interstitial Li motion in Li<sub>2</sub>CO<sub>3</sub> layer. Interstitial Li atoms are circled by a continuous blue line, while lattice Li atoms that partake in the motion are circled by a dashed blue line. The activation energy of Li hopping is reduced from 0.3 eV in bulk Li<sub>2</sub>CO<sub>3</sub> to 0.10 or 0.22 eV in the interfacial structure considered, showing that the interface assists in Li diffusion.

## Dynamics

A simulation of the finite temperature dynamics can provide insights into ion transport in the SEI, which is the rate determining step for many electrolyte-electrolyte systems.<sup>19</sup> The multiphase nature of the SEI necessitates an investigation of Li ion transport incorporating the effect of phase boundaries. To understand the effect of interface on Li ion conduction, we performed molecular dynamics simulations of the LiF-Li<sub>2</sub>CO<sub>3</sub> interfacial structure. The Li radial distribution functions at different temperatures obtained from the simulations are plotted in the Supporting Information. Previously, Mizusaki et al.<sup>52</sup> studied the conductivity of Li<sub>2</sub>CO<sub>3</sub> as a function of dopant concentration using impedance spectrometry. They found that the conductivity for pure Li<sub>2</sub>CO<sub>3</sub> along ab plane was much higher than perpendicular to it and largely due to interstitial Li ions. Fitting of their separate plots of ionic conductivity along and perpendicular to that plane to Arrhenius equation give activation energies of 0.49 and 0.62 eV respectively. The higher conductivity along ab plane may be caused by the growth along (002) plane of the crystal. Shi et al.<sup>45</sup> studied the atomistic mechanisms of Li ion transport in crystalline Li<sub>2</sub>CO<sub>3</sub>. They proposed a new mechanism by which Li ions can hop through a series of steps with low activation energy. The activation energy of the proposed *knock-off* was found to be smaller (0.3 eV) compared to the direct hopping mechanism (0.54 eV). Benitez and Seminario<sup>53</sup> studied the mechanism of Li ion conduction in the SEI components LiF, Li<sub>2</sub>O and Li<sub>2</sub>CO<sub>3</sub> using molecular dynamics based on force fields. They also inferred the *knock-off* mechanism of Li ion transport in Li<sub>2</sub>CO<sub>3</sub>. Ramasubramanian et al.<sup>54</sup> studied the conduction properties of grain boundaries between the components LiF and Li<sub>2</sub>O in the SEI. They ignored Li<sub>2</sub>CO<sub>3</sub> as a component for grain boundary conduction analysis due to the possibility of reduction in the presence of Li. We, however, consider it an important constituent for efficient Li ion transport due to strong recent evidence suggesting its presence in the SEI.<sup>18</sup>

We quantify the Li ion conduction properties of the interface through the self-diffusion coefficient of Li ions in Li<sub>2</sub>CO<sub>3</sub>. The analysis of the Car-Parrinello molecular dynamics



trajectories is done using the Suite for Analysis of MOlecular Simulations (SAMOS) package.<sup>55</sup> The diffusion coefficient  $D$  can be calculated using a linear fit of the mean squared displacement (MSD) of Li ions as a function of time  $t$ :

$$D = \frac{1}{2dt} \langle \Delta R(t)^2 \rangle \quad (2)$$

where  $d$  is the dimension ( $d = 3$  for a three-dimensional simulation) and  $\Delta R$  is the ionic displacement. Fig. 5a shows the MSD for Li, O and C ions in  $\text{Li}_2\text{CO}_3$  at 800 K and Fig. 5b shows the diagonal components of the tensor  $\mathbf{T}_{ij} = \Delta R_i \Delta R_j$  for Li ions in  $\text{Li}_2\text{CO}_3$ . Here,

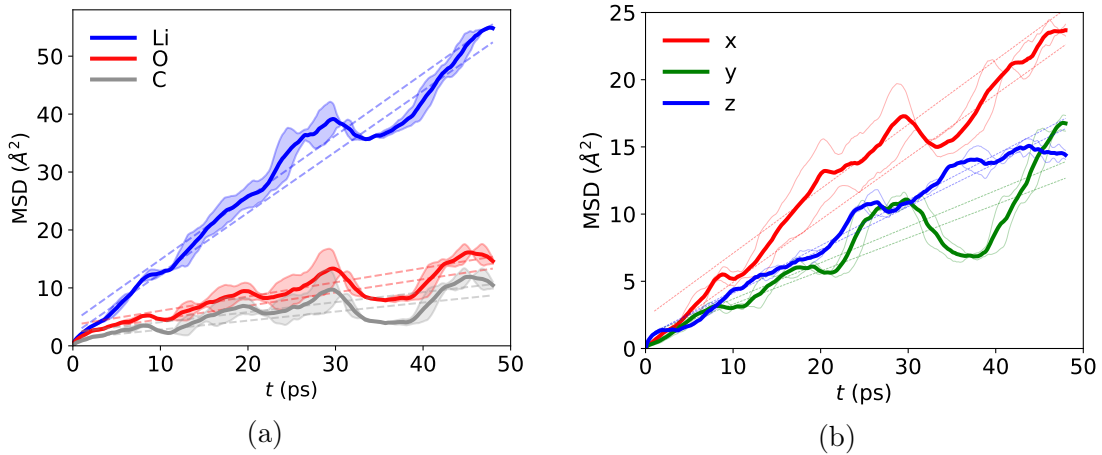


Figure 5: (a) MSD for Li, O and C ions in  $\text{Li}_2\text{CO}_3$  interfaced with LiF at 800 K. Linear fits with time are shown by dashed lines. The diffusion coefficient of Li ions is  $1.77 \times 10^{-5} \text{ cm}^2/\text{s}$ . (b) Diagonal components of the tensor  $\mathbf{T}_{ij} = \Delta R_i \Delta R_j$  for Li ions in  $\text{Li}_2\text{CO}_3$  at 800 K.

the indices  $i, j$  stand for  $\{x, y, z\}$  directions along which the displacement is calculated. The diffusive nature of Li ions is manifested by the linear increase of MSD with time. The same molecular dynamics calculations were performed at 600 and 900 K to obtain the activation energies for Li hopping. Fig. 6 shows the variation of diffusion coefficient with temperature and the fit to the Arrhenius relationship. Although the mean squared deviation along the  $x$  direction seems to be the highest at 800 K, the Li hopping along this direction also has the highest activation energy resulting in much reduced number of hops at room temperature. At 300 K, we obtain a Li ion diffusivity in  $\text{Li}_2\text{CO}_3$  equal to  $7.6 \times 10^{-11} \text{ cm}^2/\text{s}$ . This is an

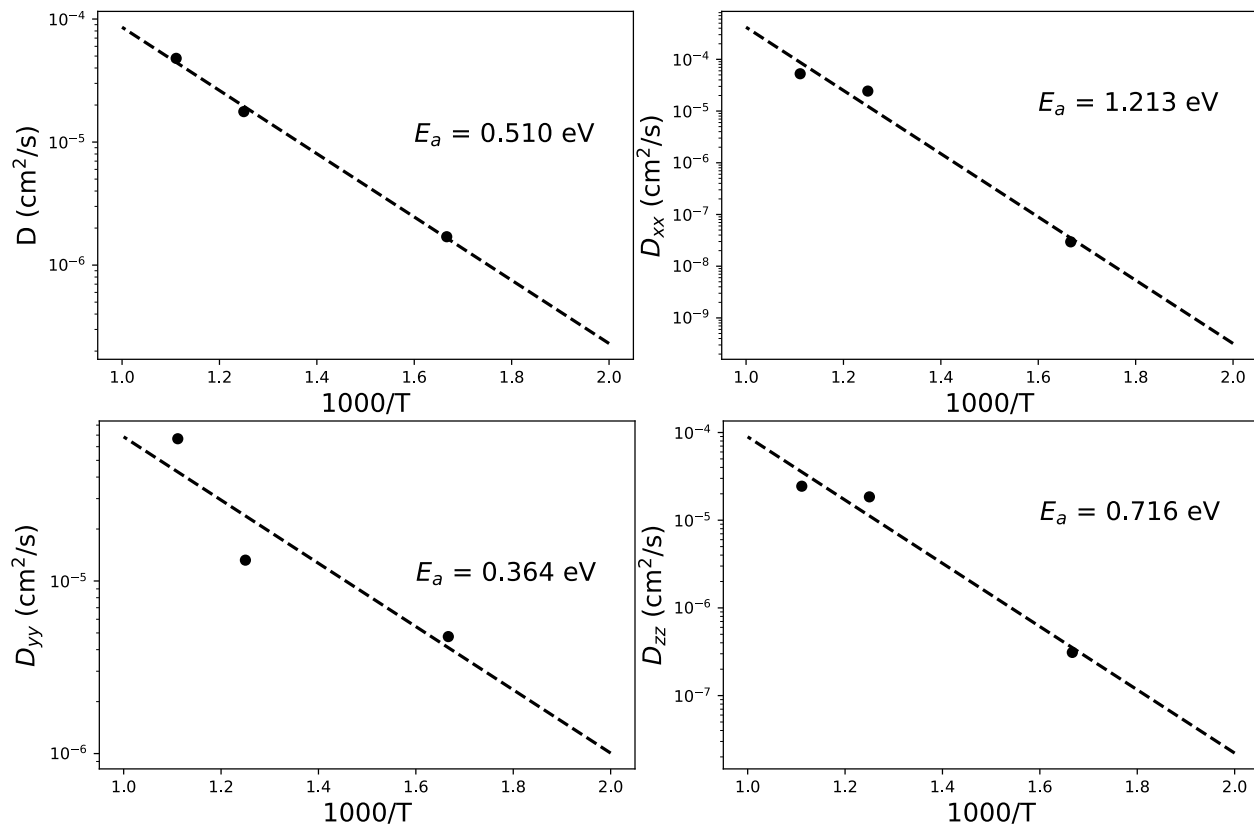


Figure 6: Variation of diffusion coefficient and the diagonal components of diffusion coefficient tensor  $D_{xx}$ ,  $D_{yy}$  and  $D_{zz}$  with temperature  $T$ . The straight line represents an Arrhenius fit. The existence of fast diffusion pathways results in a lower activation energy along the  $y$  direction.

order of magnitude higher than LiF/LiF and Li<sub>2</sub>O/Li<sub>2</sub>O grain boundaries and five times lower than LiF/Li<sub>2</sub>O phase boundary.<sup>54</sup> The differences may be due to the material or the method used to calculate diffusivity. Our interfacial structure enables us to study the layer dependent diffusivity of Li ion Li<sub>2</sub>CO<sub>3</sub>, and hence incorporate the effect of the interface ion conduction. The two Li layers closest to the interface have the highest Li ion diffusion coefficients as seen in Fig. 7. The diffusion coefficient in Li<sub>2</sub>CO<sub>3</sub> is about four orders of magnitude lower than values for a typical liquid electrolyte ( $\sim 10^{-6}\text{cm}^2/\text{s}$ ).<sup>56</sup>

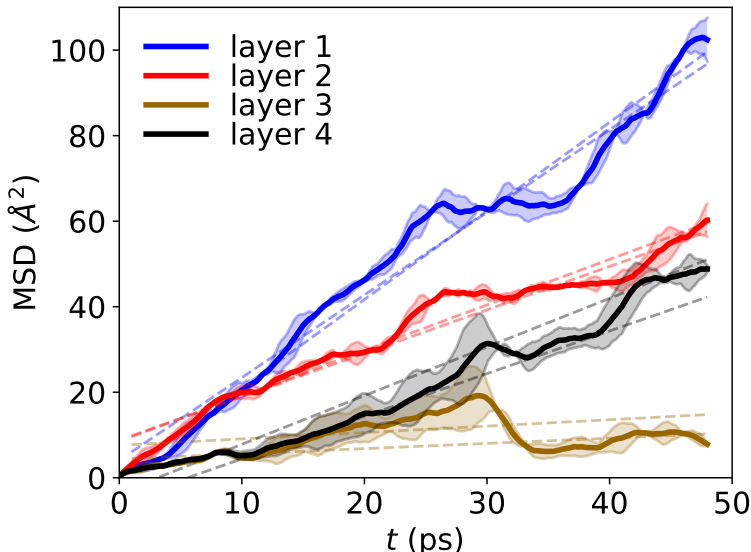


Figure 7: MSD for Li ions in Li<sub>2</sub>CO<sub>3</sub> vs time calculated layerwise at 800 K. Layer 1 is closest to the interface while layer 4 is the farthest. The layers closer to the interface have the highest MSD. The higher value for layer 4 compared to layer 3 may be due to its exposure to vacuum.

The overall activation energy for Li diffusion in Li<sub>2</sub>CO<sub>3</sub> is 0.51 eV. An overall activation energy is obtained by averaging over the different pathways for Li hopping and hence is not solely determined by the least activation energy pathway. Since the magnitude of mean squared displacement at 800 K is significant along  $x$  direction with a higher activation energy, the overall activation energy includes contributions along that pathway and is much higher than that obtained by considering only the knockoff mechanism. The activation energy for diffusion along  $y$  direction is 0.36 eV and is the lowest due to low activation energy pathways along this direction. Note that this value of self-diffusion is on par with the activation

barrier of 0.31 eV<sup>45</sup> for the optimal ionic motion pathway in bulk Li<sub>2</sub>CO<sub>3</sub> and close to 0.28 eV obtained by Iddir and Curtiss<sup>57</sup> considering motion along [010] open channels, further indicating that, on average, interfacial Li diffusion (whether mediated by interstitial atoms or otherwise) is faster than in the bulk. Solid-state NMR spectroscopy measurements revealed an activation energy for Li ion hopping in bulk Li<sub>2</sub>CO<sub>3</sub> in the range 0.78-1.34 eV.<sup>43</sup> Recent electrochemical impedance spectroscopy measurements suggested an activation energy of 0.42 eV and 0.58 eV for ionic conduction in LiF and Li<sub>2</sub>O SEI respectively.<sup>58</sup> Based on the considered LiF-Li<sub>2</sub>CO<sub>3</sub> structure (Fig. 1), we find that it is beneficial to have the plane of the lattice matched interface between LiF and Li<sub>2</sub>CO<sub>3</sub> perpendicular to the electrode-electrolyte interface to benefit from fast ion conduction along [010] direction. To further understand the mobility of Li ions in different layers of Li<sub>2</sub>CO<sub>3</sub>, we generated probability distributions of Li ions originating from Li<sub>2</sub>CO<sub>3</sub> and LiF along the axis perpendicular to the interface ( $z$ ) at 600 and 800 K as shown in Fig. S6. We observe the existence of distinct peaks in the probability distribution corresponding to the different layers in LiF and Li<sub>2</sub>CO<sub>3</sub>. There is a significant probability of Li ions from Li<sub>2</sub>CO<sub>3</sub> to migrate to LiF and vice versa at 800 and 900 K (not shown) but not at lower temperatures. However, the presence of defects might promote Li ion exchange between the two materials even at lower temperatures.

## Summary & Conclusions

We have probed the interface of canonical solid electrolyte interphase (SEI) components, LiF and Li<sub>2</sub>CO<sub>3</sub>. We studied the effects of the interface on electronic transport, Li ion conduction and defect formation in Li<sub>2</sub>CO<sub>3</sub>. Our results show that the generation of defects at the interface (Frenkel pair) requires significant energy compared to the analysis based on bulk properties. The molecular dynamics calculations reveal the Li ions starting closest to the LiF layer have the highest MSDs and hence the highest diffusion coefficients. The temperature dependence of the diffusion coefficients gives insights into the activation energies for hopping

along different directions. The lowest activation energy of 0.36 eV is obtained along the [010] direction in agreement with our results on the existence of a low activation energy pathway for Li migration in this direction in  $\text{Li}_2\text{CO}_3$ . By showing the stark difference between interfacial and bulk ionic transport phenomena, our work demonstrates that interfaces are of utmost relevance when trying to understand the SEI, “one of the most important, yet least understood,”<sup>59</sup> battery component. We note that our results rely on a crystalline structure of the multiphase SEI. Amorphous regions generated in multiphase SEI might disrupt Li ion diffusion pathways and result in a lower ionic conductivity than the single-phase SEI.<sup>58</sup> A highly heterogeneous SEI might also result in varying current densities in different regions of the electrode-electrolyte interface, potentially leading to dendrite growth in Li metal batteries. A careful design of the SEI needs to be pursued to harvest the beneficial effects of interfaces in multiphase systems.

## Acknowledgement

We thank A. Khetan for a critical reading of the manuscript. Z.A. and V.Venturi acknowledge support from the Advanced Research Projects Agency Energy (ARPA-E) under Grant DE-AR0000774. This work used the Extreme Science and Engineering Discovery Environment (XSEDE), which is supported by National Science Foundation grant number ACI-1548562.<sup>60</sup> Specifically, it used the Bridges system, which is supported by NSF award number ACI-1445606, at the Pittsburgh Supercomputing Center (PSC).<sup>61</sup>

## Supporting Information Available

The following files are available free of charge.

- supinfo.pdf: Details of electronic density of states for the pristine and defective structures

The code used for the analysis of molecular dynamics simulations is available on GitHub: <https://github.com/ahzeeshan/samos>. Relaxed configurations of the pristine and defective structures of the interface in the form of cif files are available from the GitHub repository <https://github.com/BattModels/SEI-interface>.

## References

- (1) Li, M.; Lu, J.; Chen, Z.; Amine, K. 30 years of lithium-ion batteries. *Adv. Mater.* **2018**, *30*, 1800561.
- (2) Blomgren, G. E. The development and future of lithium ion batteries. *J. Electrochem. Soc.* **2016**, *164*, A5019.
- (3) Bills, A.; Sripad, S.; Fredericks, W. L.; Singh, M.; Viswanathan, V. Performance Metrics Required of Next-Generation Batteries to Electrify Commercial Aircraft. *ACS Energy Lett.* **2020**, *5*, 663–668.
- (4) Kuhn, H.; Falter, C.; Sizmann, A. Renewable energy perspectives for aviation. Proceedings of the 3rd CEAS Air&Space Conference and 21st AIDAA Congress, Venice, Italy. 2011; pp 1249–1259.
- (5) Krishnamurthy, V.; Viswanathan, V. Beyond Transition Metal Oxide Cathodes for Electric Aviation: The Case of Rechargeable CF x. *ACS Energy Lett.* **2020**, *5*, 3330–3335.
- (6) Banerjee, A.; Wang, X.; Fang, C.; Wu, E. A.; Meng, Y. S. Interfaces and Interphases in All-Solid-State Batteries with Inorganic Solid Electrolytes. *Chem. Rev.* **2020**,
- (7) Wang, A.; Kadam, S.; Li, H.; Shi, S.; Qi, Y. Review on modeling of the anode solid electrolyte interphase (SEI) for lithium-ion batteries. *npj Comput. Mater.* **2018**, *4*.

- (8) Liang, C. C. Conduction Characteristics of the Lithium Iodide-Aluminum Oxide Solid Electrolytes. *J. Electrochem. Soc.* **1973**, *120*, 1289.
- (9) Xu, K. Nonaqueous Liquid Electrolytes for Lithium-Based Rechargeable Batteries. *Chem. Rev.* **2004**, *104*, 4303–4418.
- (10) Peled, E. The Electrochemical Behavior of Alkali and Alkaline Earth Metals in Non-aqueous Battery Systems—The Solid Electrolyte Interphase Model. *J. Electrochem. Soc.* **1979**, *126*, 2047–2051.
- (11) Zhu, Y.; He, X.; Mo, Y. Origin of Outstanding Stability in the Lithium Solid Electrolyte Materials: Insights from Thermodynamic Analyses Based on First-Principles Calculations. *ACS Appl. Mater. Interfaces* **2015**, *7*, 23685–23693.
- (12) Jin, Y. et al. Self-healing SEI enables full-cell cycling of a silicon-majority anode with a coulombic efficiency exceeding 99.9%. *Energy Environ. Sci* **2017**, *10*, 580–592.
- (13) Liu, Y.; Lin, D.; Yuen, P. Y.; Liu, K.; Xie, J.; Dauskardt, R. H.; Cui, Y. An Artificial Solid Electrolyte Interphase with High Li-Ion Conductivity, Mechanical Strength, and Flexibility for Stable Lithium Metal Anodes. *Adv. Mater.* **2017**, *29*, 1605531.
- (14) Suo, L.; Borodin, O.; Gao, T.; Olguin, M.; Ho, J.; Fan, X.; Luo, C.; Wang, C.; Xu, K. "Water-in-salt" electrolyte enables high-voltage aqueous lithium-ion chemistries. *Science* **2015**, *350*, 938–943.
- (15) Cheng, X.-B.; Zhang, R.; Zhao, C.-Z.; Wei, F.; Zhang, J.-G.; Zhang, Q. A Review of Solid Electrolyte Interphases on Lithium Metal Anode. *Adv. Sci.* **2015**, *3*, 1500213.
- (16) Zhu, Y.; Pande, V.; Li, L.; Wen, B.; Pan, M. S.; Wang, D.; Ma, Z.-F.; Viswanathan, V.; Chiang, Y.-M. Design principles for self-forming interfaces enabling stable lithium-metal anodes. *Proc. Natl. Acad. Sci. U.S.A.* **2020**, 202001923.

- (17) Verma, P.; Maire, P.; Novák, P. A review of the features and analyses of the solid electrolyte interphase in Li-ion batteries. *Electrochim. Acta* **2010**, *55*, 6332–6341.
- (18) Mozhzhukhina, N.; Flores, E.; Lundström, R.; Nyström, V.; Kitz, P. G.; Edström, K.; Berg, E. J. Direct Operando Observation of Double Layer Charging and Early Solid Electrolyte Interphase Formation in Li-Ion Battery Electrolytes. *J. Phys. Chem. Lett.* **2020**, *11*, 4119–4123.
- (19) Balbuena, P. B.; Wang, Y. *Lithium-ion batteries: solid-electrolyte interphase*; Imperial college press: London, 2004.
- (20) Jow, T. R.; Delp, S. A.; Allen, J. L.; Jones, J.-P.; Smart, M. C. Factors limiting Li<sup>+</sup> charge transfer kinetics in Li-ion batteries. *J. Electrochem. Soc.* **2018**, *165*, A361.
- (21) Leung, K.; Budzien, J. L. Ab initio molecular dynamics simulations of the initial stages of solid–electrolyte interphase formation on lithium ion battery graphitic anodes. *Phys. Chem. Chem. Phys.* **2010**, *12*, 6583.
- (22) Li, Y.; Leung, K.; Qi, Y. Computational Exploration of the Li-Electrode|Electrolyte Interface in the Presence of a Nanometer Thick Solid-Electrolyte Interphase Layer. *Acc. Chem. Res.* **2016**, *49*, 2363–2370.
- (23) Kim, K.; Siegel, D. J. Predicting Wettability and the Electrochemical Window of Lithium-Metal/Solid Electrolyte Interfaces. *ACS Appl. Mater. Interfaces* **2019**, *11*, 39940–39950.
- (24) Leung, K.; Pearse, A. J.; Talin, A. A.; Fuller, E. J.; Rubloff, G. W.; Modine, N. A. Kinetics-Controlled Degradation Reactions at Crystalline LiPON/Li<sub>x</sub>CoO<sub>2</sub> and Crystalline LiPON/Li-Metal Interfaces. *ChemSusChem* **2018**, *11*, 1956–1969.
- (25) Ramasubramanian, A.; Yurkiv, V.; Foroozan, T.; Ragone, M.; Shahbazian-Yassar, R.; Mashayek, F. Stability of Solid-Electrolyte Interphase (SEI) on the Lithium Metal



- Surface in Lithium Metal Batteries (LMBs). *ACS Appl. Energy Mater.* **2020**, *3*, 10560–10567.
- (26) Leung, K. DFT modelling of explicit solid–solid interfaces in batteries: methods and challenges. *Phys. Chem. Chem. Phys.* **2020**, *22*, 10412–10425.
- (27) Zhang, Q.; Pan, J.; Lu, P.; Liu, Z.; Verbrugge, M. W.; Sheldon, B. W.; Cheng, Y.-T.; Qi, Y.; Xiao, X. Synergetic Effects of Inorganic Components in Solid Electrolyte Interphase on High Cycle Efficiency of Lithium Ion Batteries. *Nano Lett.* **2016**, *16*, 2011–2016.
- (28) Maier, J. Ionic conduction in space charge regions. *Prog. Solid State Chem.* **1995**, *23*, 171–263.
- (29) Sata, N.; Eberman, K.; Eberl, K.; Maier, J. Mesoscopic fast ion conduction in nanometre-scale planar heterostructures. *Nature* **2000**, *408*, 946–949.
- (30) Giannozzi, P. et al. QUANTUM ESPRESSO: a modular and open-source software project for quantum simulations of materials. *J. Phys.: Condens. Matter* **2009**, *21*, 395502.
- (31) Giannozzi, P. et al. Advanced capabilities for materials modelling with Quantum ESPRESSO. *J. Phys.: Condens. Matter* **2017**, *29*, 465901.
- (32) Garrity, K. F.; Bennett, J. W.; Rabe, K. M.; Vanderbilt, D. Pseudopotentials for high-throughput DFT calculations. *Comput. Mater. Sci.* **2014**, *81*, 446–452.
- (33) Jonsson, H.; Mills, G.; Jacobsen, K. W. In *Classical and Quantum Dynamics in Condensed Phase Simulations: Proceedings of the International School of Physics*; Berne, B. J., Ciccotti, G., Coker, D. F., Eds.; World Scientific, 1998.

- (34) Enkovaara, J. et al. Electronic structure calculations with GPAW: a real-space implementation of the projector augmented-wave method. *J. Phys.: Condens. Matter* **2010**, *22*, 253202.
- (35) Larsen, A. H. et al. The atomic simulation environment—a Python library for working with atoms. *J. Phys.: Condens. Matter* **2017**, *29*, 273002.
- (36) Momma, K.; Izumi, F. VESTA 3 for three-dimensional visualization of crystal, volumetric and morphology data. *J. Appl. Crystallogr.* **2011**, *44*, 1272–1276.
- (37) Car, R.; Parrinello, M. Unified Approach for Molecular Dynamics and Density-Functional Theory. *Phys. Rev. Lett.* **1985**, *55*, 2471–2474.
- (38) Nosé, S. A unified formulation of the constant temperature molecular dynamics methods. *J. Chem. Phys.* **1984**, *81*, 511–519.
- (39) Nosé, S. A molecular dynamics method for simulations in the canonical ensemble. *Mol. Phys.* **1984**, *52*, 255–268.
- (40) Hoover, W. G. Canonical dynamics: Equilibrium phase-space distributions. *Phys. Rev. A* **1985**, *31*, 1695–1697.
- (41) Marcolongo, A.; Marzari, N. Ionic correlations and failure of Nernst-Einstein relation in solid-state electrolytes. *Phys. Rev. Mater.* **2017**, *1*.
- (42) Wyckoff, R. W. G. Crystal structures, 2nd edition. *Acta Crystallogr.* **1965**, *1*, 139.
- (43) Dunstan, M. T.; Griffin, J. M.; Blanc, F.; Leskes, M.; Grey, C. P. Ion Dynamics in Li<sub>2</sub>CO<sub>3</sub> Studied by Solid-State NMR and First-Principles Calculations. *J. Phys. Chem. C* **2015**, *119*, 24255–24264.
- (44) Idemoto, Y.; Richardson, J. W.; Koura, N.; Kohara, S.; Loong, C.-K. Crystal structure of (Li<sub>x</sub>K<sub>1-x</sub>)<sub>2</sub>CO<sub>3</sub> (x = 0, 0.43, 0.5, 0.62, 1) by neutron powder diffraction analysis. *J. Phys. Chem. Solids* **1998**, *59*, 363–376.

- (45) Shi, S.; Lu, P.; Liu, Z.; Qi, Y.; Hector, L. G.; Li, H.; Harris, S. J. Direct Calculation of Li-Ion Transport in the Solid Electrolyte Interphase. *J. Am. Chem. Soc.* **2012**, *134*, 15476–15487.
- (46) Han, F.; Westover, A. S.; Yue, J.; Fan, X.; Wang, F.; Chi, M.; Leonard, D. N.; Dudney, N. J.; Wang, H.; Wang, C. High electronic conductivity as the origin of lithium dendrite formation within solid electrolytes. *Nat. Energy* **2019**, *4*, 187–196.
- (47) Tian, H.-K.; Liu, Z.; Ji, Y.; Chen, L.-Q.; Qi, Y. Interfacial Electronic Properties Dictate Li Dendrite Growth in Solid Electrolytes. *Chem. Mater.* **2019**, *31*, 7351–7359.
- (48) Chen, Y. C.; Ouyang, C. Y.; Song, L. J.; Sun, Z. L. Electrical and Lithium Ion Dynamics in Three Main Components of Solid Electrolyte Interphase from Density Functional Theory Study. *J. Phys. Chem. C* **2011**, *115*, 7044–7049.
- (49) Gajdoš, M.; Hafner, J. CO adsorption on Cu(111) and Cu(001) surfaces: Improving site preference in DFT calculations. *Surf. Sci.* **2005**, *590*, 117–126.
- (50) Shi, S.; Qi, Y.; Li, H.; Hector, L. G. Defect Thermodynamics and Diffusion Mechanisms in Li<sub>2</sub>CO<sub>3</sub> and Implications for the Solid Electrolyte Interphase in Li-Ion Batteries. *J. Phys. Chem. C* **2013**, *117*, 8579–8593.
- (51) Fu, C.; Venturi, V.; Kim, J.; Ahmad, Z.; Ells, A. W.; Viswanathan, V.; Helms, B. A. Universal chemomechanical design rules for solid-ion conductors to prevent dendrite formation in lithium metal batteries. *Nat. Mater.* **2020**, *19*, 758–766.
- (52) Mizusaki, J.; Tagawa, H.; Saito, K.; Uchida, K.; Tezuka, M. Lithium carbonate as a solid electrolyte. *Solid State Ion.* **1992**, *53-56*, 791–797.
- (53) Benitez, L.; Seminario, J. M. Ion Diffusivity through the Solid Electrolyte Interphase in Lithium-Ion Batteries. *J. Electrochem. Soc.* **2017**, *164*, E3159–E3170.

- (54) Ramasubramanian, A.; Yurkiv, V.; Foroozan, T.; Ragone, M.; Shahbazian-Yassar, R.; Mashayek, F. Lithium Diffusion Mechanism through Solid–Electrolyte Interphase in Rechargeable Lithium Batteries. *J. Phys. Chem. C* **2019**, *123*, 10237–10245.
- (55) Suite for Analysis of Molecular Simulations. <https://github.com/ahzeeshan/samos> (accessed July 8, 2020).
- (56) Kitz, P. G.; Lacey, M. J.; Novák, P.; Berg, E. J. Operando investigation of the solid electrolyte interphase mechanical and transport properties formed from vinylene carbonate and fluoroethylene carbonate. *J. Power Sources* **2020**, *477*, 228567.
- (57) Iddir, H.; Curtiss, L. A. Li Ion Diffusion Mechanisms in Bulk Monoclinic Li<sub>2</sub>CO<sub>3</sub> Crystals from Density Functional Studies. *J. Phys. Chem. C* **2010**, *114*, 20903–20906.
- (58) Guo, R.; Gallant, B. M. Li<sub>2</sub>O Solid Electrolyte Interphase: Probing Transport Properties at the Chemical Potential of Lithium. *Chem. Mater.* **2020**, *32*, 5525–5533.
- (59) Winter, M. The solid electrolyte interphase—the most important and the least understood solid electrolyte in rechargeable Li batteries. *Z. Phys. Chem.* **2009**, *223*, 1395–1406.
- (60) Towns, J.; Cockerill, T.; Dahan, M.; Foster, I.; Gaither, K.; Grimshaw, A.; Hazelwood, V.; Lathrop, S.; Lifka, D.; Peterson, G. D.; Roskies, R.; Scott, J. R.; Wilkins-Diehr, N. XSEDE: Accelerating Scientific Discovery. *Comput. Sci. Eng.* **2014**, *16*, 62–74.
- (61) Nystrom, N. A.; Levine, M. J.; Roskies, R. Z.; Scott, J. R. Bridges: A Uniquely Flexible HPC Resource for New Communities and Data Analytics. Proceedings of the 2015 XSEDE Conference: Scientific Advancements Enabled by Enhanced Cyberinfrastructure. New York, NY, USA, 2015; pp 30:1–30:8.

Supporting Information:

Interfacial Effects on Solid Electrolyte  
Interphase in Lithium-ion Batteries

Zeeshan Ahmad,<sup>†</sup> Victor Venturi,<sup>†</sup> Hasnain Hafiz,<sup>†</sup> and Venkatasubramanian  
Viswanathan<sup>\*,†,‡</sup>

<sup>†</sup>*Department of Mechanical Engineering, Carnegie Mellon University, Pittsburgh,  
Pennsylvania 15213, USA*

<sup>‡</sup>*Department of Physics, Carnegie Mellon University, Pittsburgh, Pennsylvania 15213, USA*

E-mail: venkvis@cmu.edu

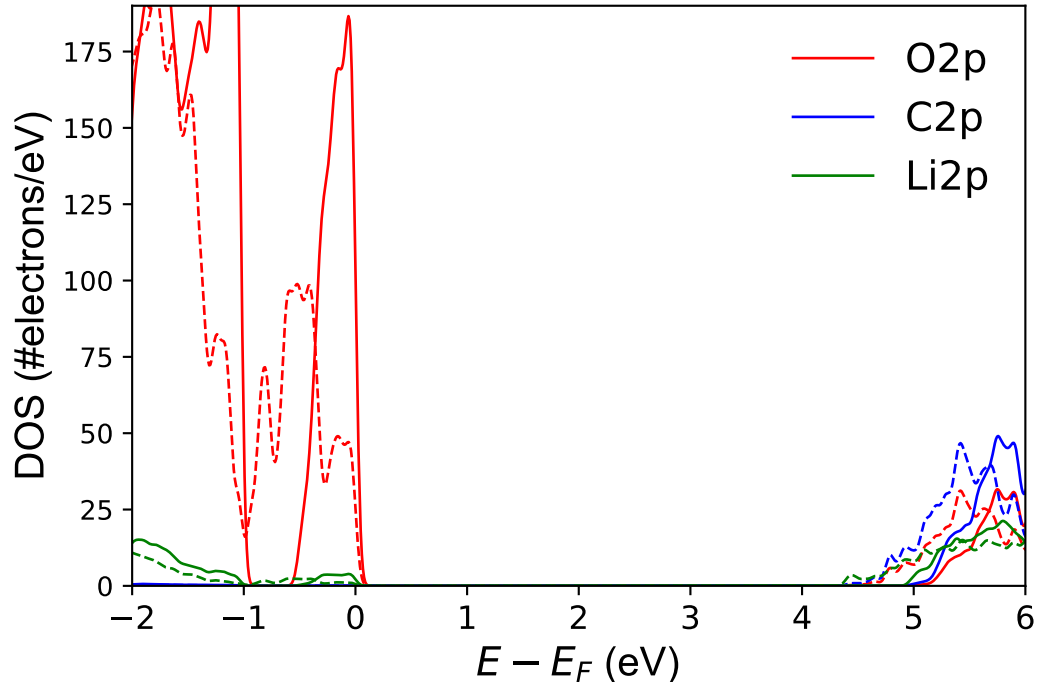


Figure S1: Comparison of electronic DOS of pristine and defective structures. The solid lines refer to pristine structure and the dashed lines refer to the defective structure. The Fermi level  $E_F$  is set to VBM.

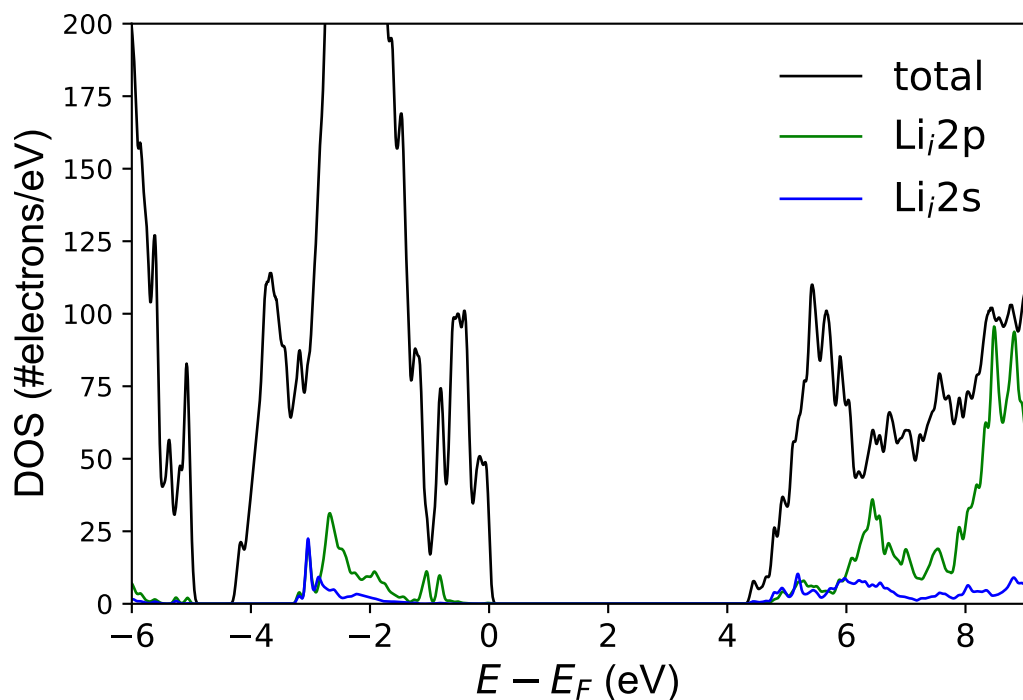


Figure S2: Electronic states of interstitial Li ( $\text{Li}_i$ ) at the  $\text{LiF-Li}_2\text{CO}_3$  interface. The  $\text{Li}_i$  interstitial DOS has been exaggerated by multiplying the no of states/eV with 100.

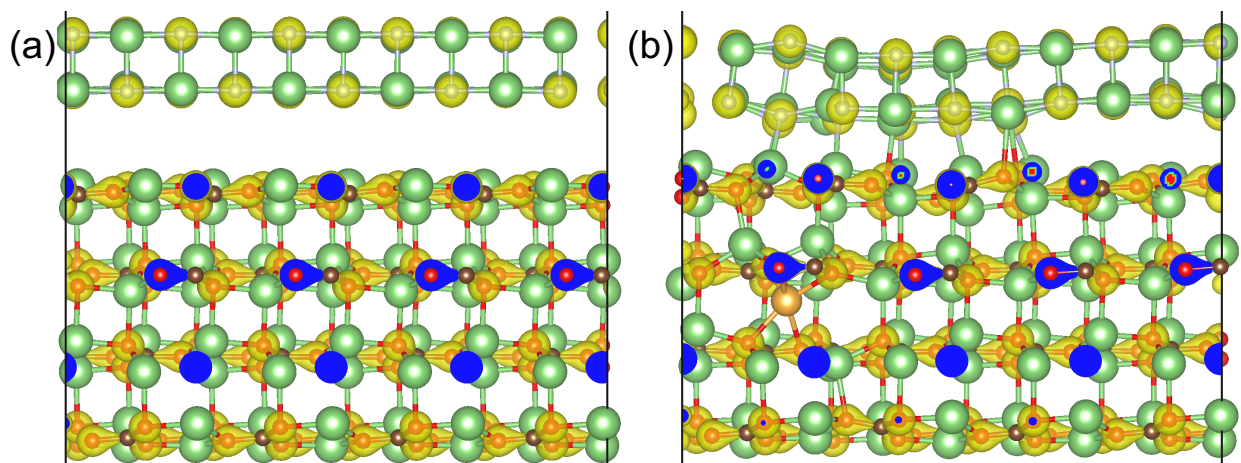


Figure S3: Electron density for the (a) pristine and (b) defective interfacial structure between  $\text{LiF}$  and  $\text{Li}_2\text{CO}_3$ . The  $\text{Li}_i$  interstitial defect in  $\text{Li}_2\text{CO}_3$  is shown in yellow.

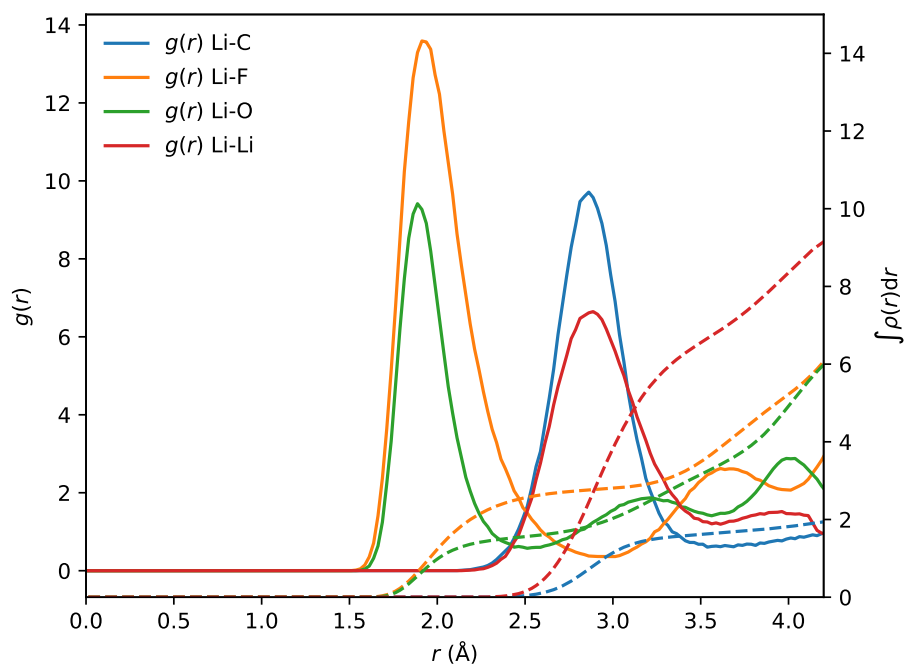


Figure S4: Radial distribution function  $g(r)$  for the LiF-Li<sub>2</sub>CO<sub>3</sub> interfacial structure at 600 K.

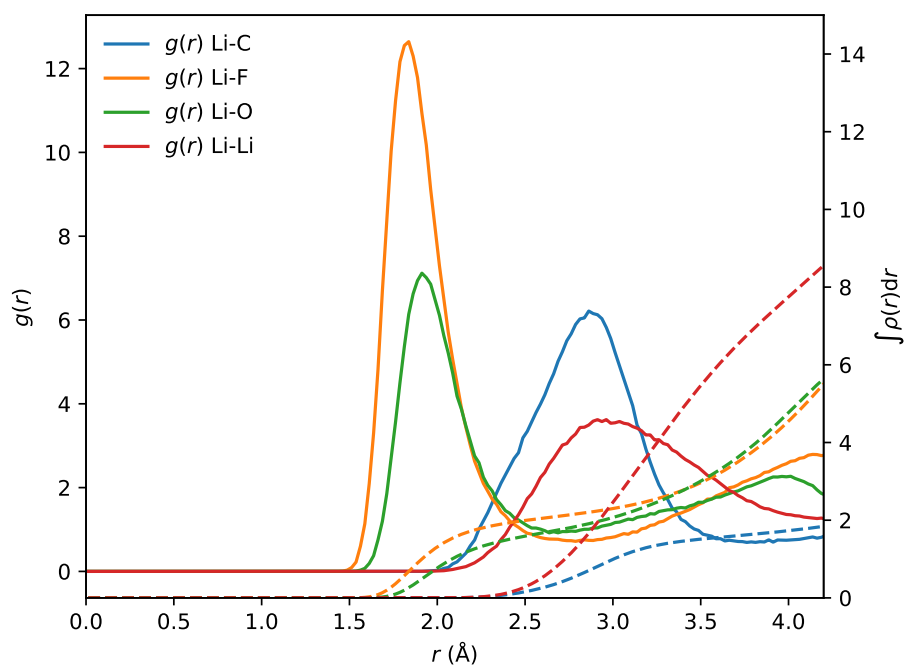


Figure S5: Radial distribution function  $g(r)$  for the LiF-Li<sub>2</sub>CO<sub>3</sub> interfacial structure at 800 K.



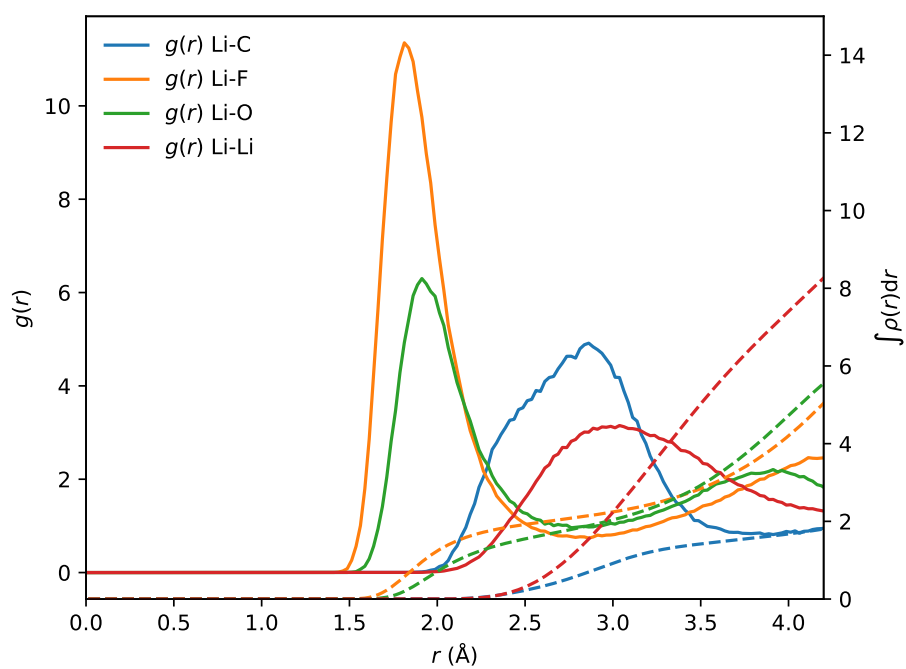


Figure S6: Radial distribution function  $g(r)$  for the LiF-Li<sub>2</sub>CO<sub>3</sub> interfacial structure at 900 K.

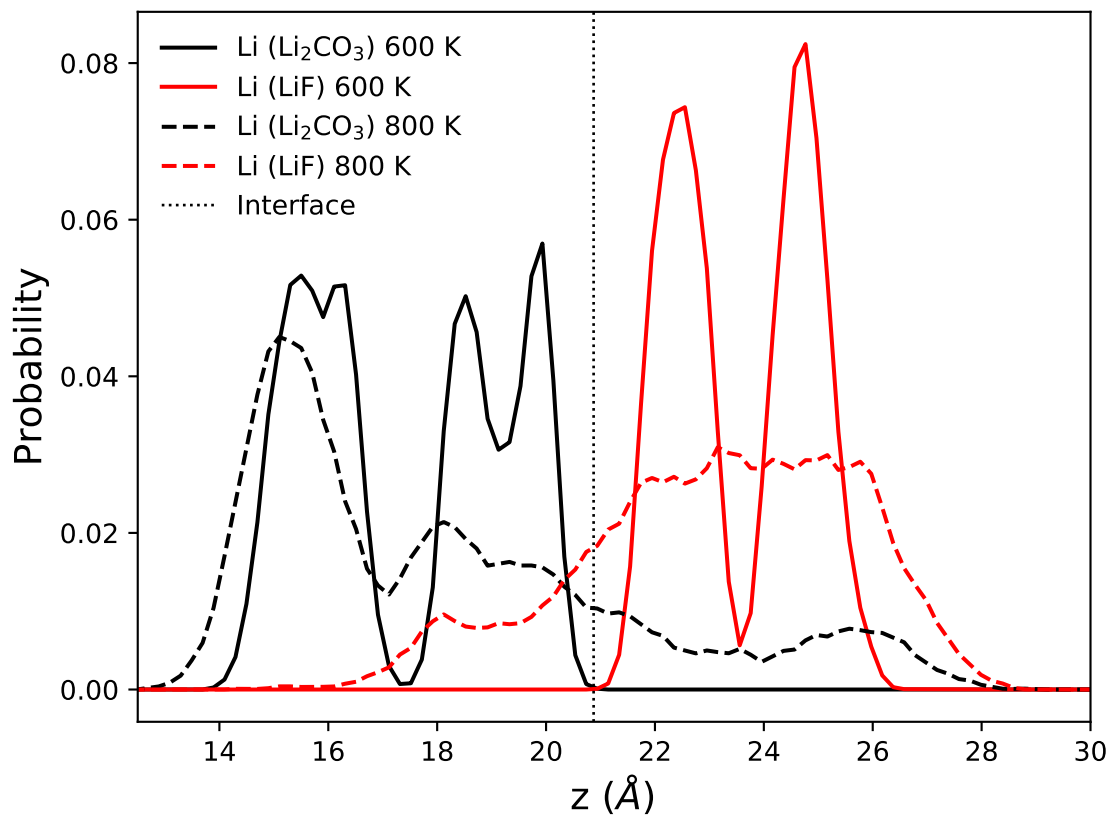


Figure S7: Probability density for the position of a Li ion as a function of the direction perpendicular to the interface  $z$  at 600 and 800 K. The initial position of the interface, located near  $z = 21$  Å is shown with a dotted line. The black and red lines represent Li initially in the Li<sub>2</sub>CO<sub>3</sub> and LiF phases respectively. The plot demonstrates significant exchange of Li ions between LiF and Li<sub>2</sub>CO<sub>3</sub> at 800 K which is not present at 600 K.

# Graphical TOC Entry

